SEPTEMBER 18 2025

Comparative study of microphone arrays comprising omnidirectional and first-order directional microphones applied to remote virtual sensing

Achilles Kappis ; Jordan Cheer

Proc. Mtgs. Acoust. 56, 055003 (2025)
https://doi.org/10.1121/2.0002095

Volume 56 http://acousticalsociety.org/

ASA/ICA 2025 New Orleans

188th Meeting of the Acoustical Society of America
joint with
25th International Congress on Acoustics

New Orleans, Louisiana
18-23 May 2025

Signal Processing in Acoustics: Paper 1pSPa4

Comparative study of microphone arrays comprising omnidirectional and first-order directional microphones applied to remote virtual sensing

Achilles Kappis and Jordan Cheer
Institute of Sound and Vibration Research, University of Southampton, Southampton, Hampshire, SO17 1BJ, UNITED KINGDOM; axilleaz@protonmail.com; ak1a23@soton.ac.uk; A.Kappis@soton.ac.uk; j.cheer@soton.ac.uk

Virtual sensing techniques have been variously investigated within the context of active noise control, and it has been demonstrated that accurate estimation is critical to active control performance. The current work aims to compare the performance and robustness of monitoring microphone arrays used for virtual sensing, comprising omnidirectional pressure sensors and microphones with first-order directivity characteristics. Configurations with the standard first-order directivity patterns, dipole, cardioid, hyper-cardioid and super-cardioid, and their combinations are investigated and compared to conventional arrays with omnidirectional microphones. The estimation is performed through the formulation of observation filters that project the measured responses to the estimate of the sound field at the position of virtual microphones, using the Remote Microphone Technique. The study explores the performance and robustness of the monitoring configurations when used to estimate the pressure in a diffuse sound field. A closed-form formulation of the problem is presented, and simulations are performed to validate the theoretical results.

Proceedings of Meetings on Acoustics, Vol. 56, 055003 (2025); https://doi.org/10.1121/2.0002095.

1. INTRODUCTION

Virtual sensing (VS) methods have been applied across various scientific disciplines to estimate parameters at remote locations where sensor placement is impractical.[1,2] Despite variations in implementation, VS methods offer a compelling approach for parameter estimation at locations distant from sensor positions. In active noise control (ANC), VS techniques improve local sound field control[2] by estimating sound field parameters at the required control position. Various studies have shown that ANC systems embedding virtual sensing achieve improved attenuation performance compared to conventional systems, particularly in applications like the active headrest.[3,4] However, the accuracy of sound field parameter estimation remains critical and can limit control performance.[5]

Conventionally, omnidirectional sensors have been employed to sample sound fields and extrapolate the pressure at remote locations.[2–4] However, findings indicate that incorporating pressure gradient information significantly enhances attenuation performance,[6–8] observability[9–11] and estimation accuracy,[12,13] providing an expansion to the effective area of control. Pressure gradient can be incorporated through distinct particle velocity sensors[6] or via closely-spaced pressure microphones.[14] Both methods provide accurate estimates of pressure, pressure gradient and total acoustic energy[15,16] at a distinct point in a sound field.

The current study investigates the estimation performance of monitoring configurations comprising first-order directional microphones[17] embedded in a diffuse sound field. The remote microphone technique (RMT) VS method[2] is employed to estimate the sound field, where the estimate at a virtual microphone position is calculated as a linear combination of monitoring microphone signals encoded by an observation filter. Unlike previous studies[6,12,13] that utilised separate sensors for pressure and pressure gradient information, this study employs first-order microphone signals that result from a weighted combination of the two quantities. Additionally, the directionality of the microphones introduces an extra degree of freedom through their orientation.

Initially, a closed-form solution for calculating the estimation performance of the VS system in a diffuse field based on past work[17,18] is generalised using vector algebra. The performance of two-microphone systems is evaluated numerically based on this formulation. Subsequently, the sensitivity of the configurations to uncertainties is investigated, and the robustness of the microphone pairs against spatially uncorrelated noise is explored under varying noise conditions.

2. REMOTE MICROPHONE VIRTUAL SENSING WITH FIRST-ORDER DIRECTIONAL MICROPHONES

A. REMOTE MICROPHONE VIRTUAL SENSING

The generalised block diagram of a VS system employing the RMT is shown in Fig. 1. In the general case, N_v sources with complex strengths $\boldsymbol{v} = [v_1, v_2, \ldots, v_{N_\mathrm{v}}]^\mathrm{T}$, where $[\cdot]^\mathrm{T}$ denotes transposition, generate the responses at N_m monitoring microphones, $\boldsymbol{d}_\mathrm{m} = \left[d_{\mathrm{m}_1}, d_{\mathrm{m}_2}, \ldots, d_{\mathrm{m}_{N_\mathrm{m}}}\right]^\mathrm{T}$, and N_e virtual microphones, $\boldsymbol{d}_\mathrm{e} = \left[d_{\mathrm{e}_1}, d_{\mathrm{e}_2}, \ldots, d_{\mathrm{e}_{N_\mathrm{m}}}\right]^\mathrm{T}$. The measured responses are expressed as

$$\boldsymbol{d}_\mathrm{m} = \boldsymbol{P}_\mathrm{m}\boldsymbol{v} \tag{1a}$$

$$\boldsymbol{d}_\mathrm{e} = \boldsymbol{P}_\mathrm{e}\boldsymbol{v}, \tag{1b}$$

where $\boldsymbol{P}_\mathrm{m} \in \mathbb{C}^{N_\mathrm{m} \times N_\mathrm{v}}$ and $\boldsymbol{P}_\mathrm{e} \in \mathbb{C}^{N_\mathrm{e} \times N_\mathrm{v}}$ are the frequency response functions (FRFs) between the disturbance sources and the monitoring and virtual microphones, respectively. The frequency dependence is suppressed for notational convenience.

The estimated sound field at the virtual microphone positions, $\hat{\boldsymbol{d}}_\mathrm{e}$, where $[\hat{\cdot}]$ denotes an estimated quantity, is calculated as a linear combination of the monitoring signals, $\boldsymbol{d}_\mathrm{m}$, encoded by the observation filter $\hat{\boldsymbol{O}}$.

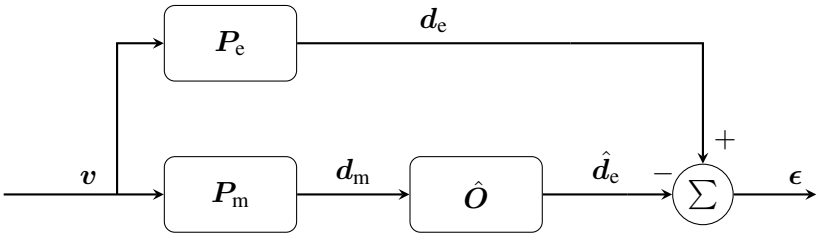

Figure 1: Generalised block diagram of a virtual sensing system. The sound field measured by the error microphones, d_e, are estimated from the signals measured at the monitoring microphones, d_m, as the linear combination described by the observation filter $\hat{O}$, to provide the estimated sound field at the virtual locations, $\hat{d}_e$.

The estimation error is the difference between the true and estimated disturbance fields, given by

$$\boldsymbol{\epsilon} = \boldsymbol{d}_\mathrm{e} - \hat{\boldsymbol{d}}_\mathrm{e} = \boldsymbol{d}_\mathrm{e} - \hat{\boldsymbol{O}}\boldsymbol{d}_\mathrm{m} = \boldsymbol{P}_\mathrm{e}\boldsymbol{v} - \hat{\boldsymbol{O}}\boldsymbol{P}_\mathrm{m}\boldsymbol{v}. \tag{2}$$

The optimal solution, in the least squares sense, is obtained by minimising the mean squared estimation error. Assuming the source signals are realisations of a wide-sense stationary random process, the cost function is given by[19]

$$J_2 = S_{\epsilon\epsilon} = \mathrm{E}\left[\boldsymbol{\epsilon}^\mathrm{H}\boldsymbol{\epsilon}\right] = \mathrm{E}\left[\mathrm{tr}\left\{\boldsymbol{\epsilon}\boldsymbol{\epsilon}^\mathrm{H}\right\}\right] = \mathrm{tr}\left\{\boldsymbol{S}_\mathrm{ee} - \boldsymbol{S}_\mathrm{me}\hat{\boldsymbol{O}}^\mathrm{H} - \hat{\boldsymbol{O}}\boldsymbol{S}_\mathrm{me}^\mathrm{H} + \hat{\boldsymbol{O}}\boldsymbol{S}_\mathrm{mm}\hat{\boldsymbol{O}}^\mathrm{H}\right\}, \tag{3}$$

where $\mathrm{E}[\,\cdot\,]$ denotes the expectation operator, $\mathrm{tr}\{\,\cdot\,\}$ the trace of a matrix, $[\,\cdot\,]^\mathrm{H}$ Hermitian transposition, and $S_{\epsilon\epsilon}$ the power spectral density (PSD) of the error signal. The quantities $\boldsymbol{S}_\mathrm{ee}$ and $\boldsymbol{S}_\mathrm{mm}$ are the PSD matrices of the virtual and monitoring microphones, respectively, and $\boldsymbol{S}_\mathrm{me}$ is the cross spectral density (CSD) matrix between the monitoring and virtual microphone signals. The solution to Eq. (3) is[2,19]

$$\hat{\boldsymbol{O}}_\mathrm{opt} = \boldsymbol{S}_\mathrm{me}\left(\boldsymbol{S}_\mathrm{mm} + \beta\boldsymbol{I}\right)^{-1}, \tag{4}$$

where $[\,\cdot\,]^{-1}$ denotes matrix inversion, $\boldsymbol{I}$ is an $N_\mathrm{m}\times N_\mathrm{m}$ identity matrix, and β is a non-negative regularisation parameter used to constrain the magnitude of the filter weights. Regularisation of this form can reduce sensitivity to uncertainties and is equivalent to introducing uncorrelated noise of strength β to the monitoring microphone responses.[20]

The estimation performance is determined by the coherence between the monitoring and virtual microphone signals.[13,21] The squared multiple coherence between the monitoring microphone signals and the signal of a single virtual microphone in matrix form is[21]

$$\gamma^2 = \frac{\boldsymbol{S}_\mathrm{me}\boldsymbol{S}_\mathrm{mm}^{-1}\boldsymbol{S}_\mathrm{me}^\mathrm{H}}{S_\mathrm{ee}}. \tag{5}$$

The metric used in this work to quantify estimation accuracy is the normalised mean squared estimation error (NMSE), calculated as[3,5,19]

$$L_\mathrm{e} = 10\log_{10}\left(\frac{\mathrm{E}\left[\boldsymbol{\epsilon}^\mathrm{H}\boldsymbol{\epsilon}\right]}{S_\mathrm{ee}}\right) = 10\log_{10}\left(\frac{S_{\epsilon\epsilon}}{S_\mathrm{ee}}\right) = 10\log_{10}\left(1-\gamma^2\right). \tag{6}$$

B. FIRST ORDER DIFFERENTIAL MICROPHONES IN A DIFFUSE SOUND FIELD

To calculate the coherence between monitoring and virtual microphones, as defined in Eq. (5), it is necessary to know the correlation between monitoring microphones and between the monitoring and virtual

microphones. Closed-form solutions for the correlation between two first-order directional microphones are available for isotropic[17,18] fields. This section presents a formulation using vector algebra, which can be applied to arbitrary microphone configurations.

The response of a first-order directional microphone is formed as the weighted combination of pressure and pressure gradient along the microphone's "look direction". The ideal, frequency-independent directional response is axisymmetric and is expressed as

$$B(\theta) = a + (1-a)\cos(\theta) = a + b\cos(\theta) = a + b\,\bar{\boldsymbol{u}} \cdot \bar{\boldsymbol{k}} = a + \boldsymbol{u} \cdot \bar{\boldsymbol{k}}, \tag{7}$$

where θ is the angle between the microphone's look direction and the incident sound field, and $a \in [0, 1]$ provides the relative weight of the pressure and pressure gradient components. The symbol $[\circ \cdot \circ]$ denotes the dot product, $\boldsymbol{u} = b\bar{\boldsymbol{u}}$ is the particle velocity vector associated with the microphone response, and $\bar{\boldsymbol{u}}$ and $\bar{\boldsymbol{k}}$ are unit vectors indicating the microphone's orientation and the direction of arrival of the sound field (normalised wavevector), respectively. The microphone directivities used in this work are presented in Table 1, which includes their directional responses, the angle at which the response is null, and the associated a parameter.

Table 1: Constraint angles and the corresponding a weights associated with the responses of ideal first-order microphones.

Microphone response	$\boldsymbol{\phi}$ **(degrees)**	$\boldsymbol{a}$
Cardioid	180	0.5
Supercardioid	125	0.37
Hypercardioid	110	0.25
Figure-of-Eight	90	0

In a diffuse field, the orthogonal particle velocity components between two positions are zero,[22] so the correlation between the particle velocity at two spaced microphone positions is due solely to their collinear components. The magnitude of these components determines the degree of correlation and can be calculated as the dot product of the particle velocity vectors $\boldsymbol{u}$ as

$$\mathrm{E}[\boldsymbol{u}_1 \boldsymbol{u}_2^*] \sim \boldsymbol{u}_1 \cdot \boldsymbol{u}_2 = b_1 b_2 \left(\bar{\boldsymbol{u}}_1 \cdot \bar{\boldsymbol{u}}_2\right). \tag{8}$$

The correlation between two microphones can be analysed in terms of their components parallel to the displacement vector $\boldsymbol{r}$ connecting the microphones and its complement with respect to the total correlation. The particle velocity components parallel and orthogonal to $\boldsymbol{r}$ are illustrated in Fig. 2a. The degree of correlation between the components parallel to $\boldsymbol{r}$ can be calculated as their dot product to give

$$b_{\parallel} = \boldsymbol{b}_{1_{\parallel}} \cdot \boldsymbol{b}_{2_{\parallel}} = \left[b_1 \left(\bar{\boldsymbol{u}}_1 \cdot \bar{\boldsymbol{r}}\right) \bar{\boldsymbol{r}}\right] \cdot \left[b_2 \left(\bar{\boldsymbol{u}}_2 \cdot \bar{\boldsymbol{r}}\right) \bar{\boldsymbol{r}}\right] = b_1 b_2 \left(\bar{\boldsymbol{u}}_1 \cdot \bar{\boldsymbol{r}}\right) \left(\bar{\boldsymbol{u}}_2 \cdot \bar{\boldsymbol{r}}\right) = b_{1_{\parallel}} b_{2_{\parallel}}, \tag{9}$$

where $\bar{\boldsymbol{r}} = \boldsymbol{r}/\|\boldsymbol{r}\|$ is the unit vector along $\boldsymbol{r}$, and $\|\cdot\|$ denotes the magnitude of a vector. The magnitude of the particle velocity components parallel to $\boldsymbol{r}$ is given by $b_{\mathrm{n}_{\parallel}} = b_{\mathrm{n}} \left(\bar{\boldsymbol{u}} \cdot \bar{\boldsymbol{r}}\right)$. The complement of the dot product of Eq. (9) with respect to the total correlation of Eq. (8) gives the degree of correlation of the particle velocity components orthogonal to $\boldsymbol{r}$ as

$$b_{\perp} = \boldsymbol{b}_{1_{\perp}} \cdot \boldsymbol{b}_{2_{\perp}} = \left(\boldsymbol{u}_1 \cdot \boldsymbol{u}_2\right) - \left(\boldsymbol{b}_{1_{\parallel}} \cdot \boldsymbol{b}_{2_{\parallel}}\right) = b_1 b_2 \left[\left(\bar{\boldsymbol{u}}_1 \times \bar{\boldsymbol{r}}\right) \cdot \left(\bar{\boldsymbol{u}}_2 \times \bar{\boldsymbol{r}}\right)\right], \tag{10}$$

where $[\circ \times \circ]$ denotes the cross product. To derive Eq. (10), the total correlation term was multiplied by $\bar{\boldsymbol{r}} \cdot \bar{\boldsymbol{r}}$, and the identity $(\boldsymbol{x} \times \boldsymbol{y}) \cdot (\boldsymbol{w} \times \boldsymbol{z}) = (\boldsymbol{x} \cdot \boldsymbol{w})(\boldsymbol{y} \cdot \boldsymbol{z}) - (\boldsymbol{x} \cdot \boldsymbol{z})(\boldsymbol{y} \cdot \boldsymbol{w})$ was applied. The degree of correlation between the two particle velocity components orthogonal to the line joining the microphones is the collinear component of the two velocity vectors normal to the planes formed by $\bar{\boldsymbol{u}}$ and $\bar{\boldsymbol{r}}$.

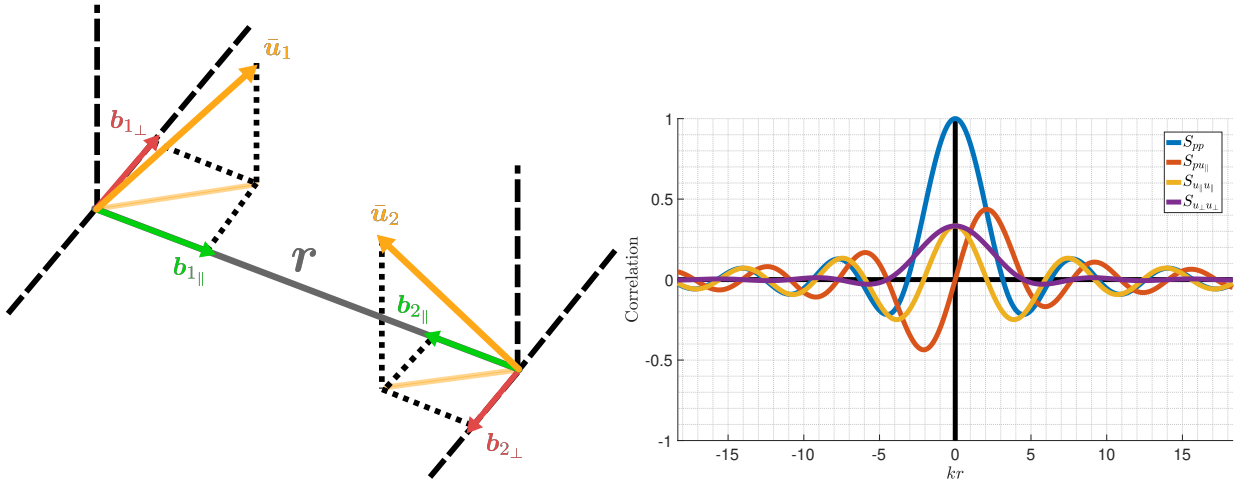

(a) Particle velocity components for a pair of microphones. *(b) Spatial correlation functions.*

Figure 2: (a) diagram of two randomly orientated microphones with the particle velocity components parallel to the displacement vector r that joins them and perpendicular to the plane formed by r and the orientation vectors $\bar{u}_n$ and (b) The spatial correlation functions in a diffuse field.

The correlation functions between pressure, pressure and particle velocity, and particle velocity components in a diffuse field are given by Eq. (11)[22] and are plotted in Fig. 2b against kr, where k is the wavenumber and $r = \|\boldsymbol{r}\|$ is the distance between points in space.

$$S_{\mathrm{pp}}(kr) = \frac{\sin(kr)}{kr} = \mathrm{sinc}(kr) \tag{11a}$$

$$S_{\mathrm{pu}_\parallel}(kr) = \frac{\sin(kr) - kr\cos(kr)}{(kr)^2} \tag{11b}$$

$$S_{\mathrm{u}_\perp\mathrm{u}_\perp}(kr) = \frac{\sin(kr) - kr\cos(kr)}{(kr)^3} \tag{11c}$$

$$S_{\mathrm{u}_\parallel\mathrm{u}_\parallel}(kr) = \frac{(kr)^2\sin(kr) + (2kr)\cos(kr) - 2\sin(kr)}{(kr)^3}. \tag{11d}$$

S_{pp} denotes the pressure correlation between two points, $S_{\mathrm{pu}_\parallel}$ denotes the correlation between pressure and particle velocity along $\boldsymbol{r}$, and $S_{\mathrm{u}_\perp\mathrm{u}_\perp}$ and $S_{\mathrm{u}_\parallel\mathrm{u}_\parallel}$ denote the correlations between particle velocity components orthogonal and parallel to $\boldsymbol{r}$, respectively.

The total correlation between the two microphones, which is equal to their CSD, is the sum of the weighted correlations of Eq. (11), with the weights calculated by Eq. (9) and Eq. (10). The form of the correlation has been calculated in past studies[17,18] and introducing the particle velocity weights, it is expressed as

$$S_{12}(kr) = \mathrm{E}[B_1 B_2^*] = a_1 a_2 S_{\mathrm{pp}}(kr) + b_\parallel S_{\mathrm{u}_\parallel\mathrm{u}_\parallel}(kr) + b_\perp S_{\mathrm{u}_\perp\mathrm{u}_\perp}(kr) + \mathrm{j}\left(a_1 b_{2_\parallel} + a_2 b_{1_\parallel}\right) S_{\mathrm{pu}_\parallel}(kr), \tag{12}$$

where $\mathrm{j} = \sqrt{-1}$ denotes the imaginary unit. The imaginary part of the correlation results from the quadrature between pressure and particle velocity.[18]

The PSD of the microphones can be calculated using Eq. (12) by setting $a_1 = a_2$ and $r = 0$. Noting that $S_{\mathrm{pu}_\parallel}(0) = 0$ and $S_{\mathrm{u}_\parallel}(0) = S_{\mathrm{u}_\perp}(0) = 1/3$ (applying L'Hôspital's rule),[22] and that $b_\parallel + b_\perp = \boldsymbol{u}_1 \cdot \boldsymbol{u}_2$, the PSD is obtained as[17,18]

$$S_{\mathrm{n}} = \mathrm{E}[B_{\mathrm{n}} B_{\mathrm{n}}^*] = a_{\mathrm{n}}^2 + \frac{b_{\mathrm{n}}^2}{3}. \tag{13}$$

It is noted that the PSD is constant and does not depend on frequency.

Equations (12) and (13) enable the calculation of the components of $\boldsymbol{S}_{\mathrm{mm}}$ if the position and orientation of the microphones are known. To calculate the elements of $\boldsymbol{S}_{\mathrm{me}}$, the correlation between the directional microphones and the pressure at the virtual microphone position can be calculated by setting $a_2 = 1$ and $b_2 = 0$ in Eq. (12) resulting in

$$S_{\mathrm{me_n}} = a_{\mathrm{n}} S_{\mathrm{pp}}(kr_{\mathrm{ne}}) + \mathrm{j} b_{\mathrm{ne}_\parallel} S_{\mathrm{pu}_\parallel}(kr_{\mathrm{ne}}), \tag{14}$$

where r_{ne} is the distance between the virtual microphone and the nth monitoring microphone, $b_{\mathrm{ne}_\parallel} = \bar{\boldsymbol{u}} \cdot \bar{\boldsymbol{r}}_{\mathrm{e}}$ is the particle velocity component parallel to the line connecting the nth monitoring microphone and the virtual microphone, and $\bar{\boldsymbol{r}}_{\mathrm{e}}$ is the normalised displacement vector of the virtual microphone.

3. PERFORMANCE OF A TWO-MICROPHONE SYSTEM

In this section, the estimation performance of a VS system comprising two first-order microphones is evaluated on a $1\,\mathrm{m} \times 1\,\mathrm{m}$ grid of 81×81 virtual microphones in the $x - y$ plane. The grid is centred at the origin, with the two microphones positioned along the y-axis, $r = 0.2\,\mathrm{m}$ apart. The frequency of the diffuse sound field is $f = 200\,\mathrm{Hz}$, which results in $kr \approx 0.73$.

It has been demonstrated that closely spaced pressure sensors improve estimation accuracy along their axis by utilising pressure gradient information.[6,8,12] To compare the performance of arrays combining omnidirectional and directional microphones, the monitoring microphones are orientated in opposite directions along the y-axis, aligning their particle velocity vectors $\boldsymbol{u}$ with the axis of the omnidirectional microphones. Figure 3 illustrates the estimation NMSE for all possible combinations of first-order directional and omnidirectional microphones. The titles denote the microphone combinations and the sum of the pressure weights in the system. Solid and dashed lines indicate areas where the error is less than $-20\,\mathrm{dB}$ and $-10\,\mathrm{dB}$, respectively.

From the results presented in Fig. 3, it can be seen that systems comprising only directional microphones do not produce a $-20\,\mathrm{dB}$ estimation zone. The contribution of pressure gradient components to the coherence is relatively small and diminishes quickly with both distance and the angle between the microphone orientation and the line connecting the monitoring and virtual microphones. The pressure gradient does not significantly enhance coherence to compensate for the reduced pressure contribution, resulting in errors that do not reach the $-20\,\mathrm{dB}$ threshold for arrays consisting solely of directional microphones. Notably, while a cardioid pair and the combination of an omnidirectional and a figure-of-eight microphone have equal total pressure contributions, only the use of a pressure microphone results in the generation of a $-20\,\mathrm{dB}$ zone, highlighting the importance of localised pressure measurements for accurate estimation. However, incorporating pressure gradient information can extend the estimation zones along its axis, with the extension increasing with the pressure gradient contribution.

The orientation of directional microphones introduces an additional parameter per microphone. To investigate the behaviour of estimation zone extension along the microphone orientations, the first microphone of each pair is orientated at angles of $0°$, $45°$ and $90°$ with the x-axis, while the second microphone is rotated through a full circle. Figure 4 displays the size of the $-10\,\mathrm{dB}$ estimation zones generated for each microphone orientation.

From the results presented in Figure 4, it can be seen that pairs consisting only of directional microphones generate estimation zones only when orientated in opposite directions. Reducing the total pressure

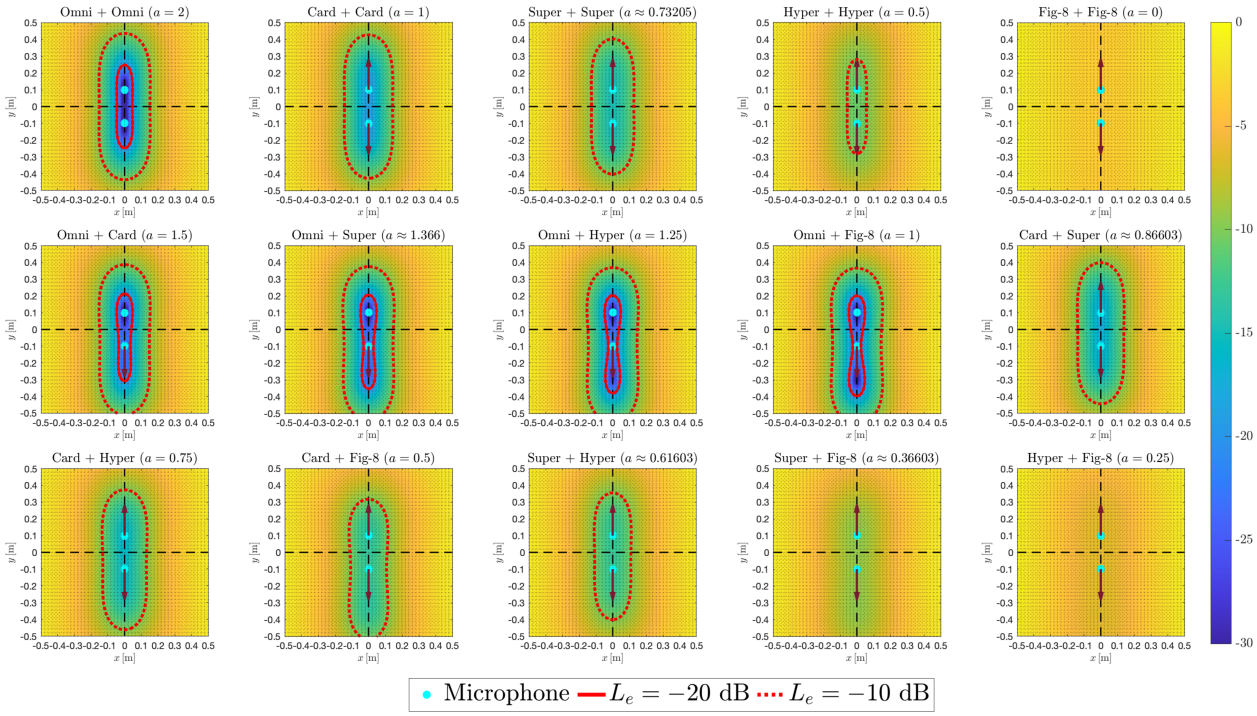

Figure 3: Spatial distribution of the estimation error for all possible combinations of first-order microphones in a diffuse sound field of frequency $f = 200$ Hz. The solid lines (–) denote the area for which $L_e \leq -20$ dB and the dashed lines (- -) enclose the area where $L_e \leq -10$ dB.

contribution decreases the angular range over which a zone is produced. Configurations with one omnidirectional microphone achieve the largest zone extension when the directional microphone is parallel to the array axis. Investigating the shape of the estimation zones of the pairs with a single omnidirectional microphone can provide further insight. Figure 5 illustrates the spatial error distribution for the four configurations with one pressure sensor when the directional microphone is orientated at $-45°$ to the x-axis. The zones are concentrated around the omnidirectional microphone and extend along the orientation of the directional microphone, providing pressure gradient information. Increasing the pressure weight of the directional microphone enlarges the zone towards its position, while a higher pressure gradient contribution elongates the zone along its axis.

4. ROBUSTNESS TO NOISE

A. CONDITION NUMBER OF MICROPHONE PAIRS

It has been shown that when the monitoring microphone responses are strongly correlated, the PSD matrix can become ill-conditioned, increasing the sensitivity of the system to practical uncertainties.[3,5] Directional microphones, due to their spatial selectivity, exhibit decreased correlation, potentially improving the system's robustness. The metric used to quantify the sensitivity of a configuration to uncertainties is the condition number of the monitoring microphone PSD matrix, which is inverted in the calculation of the

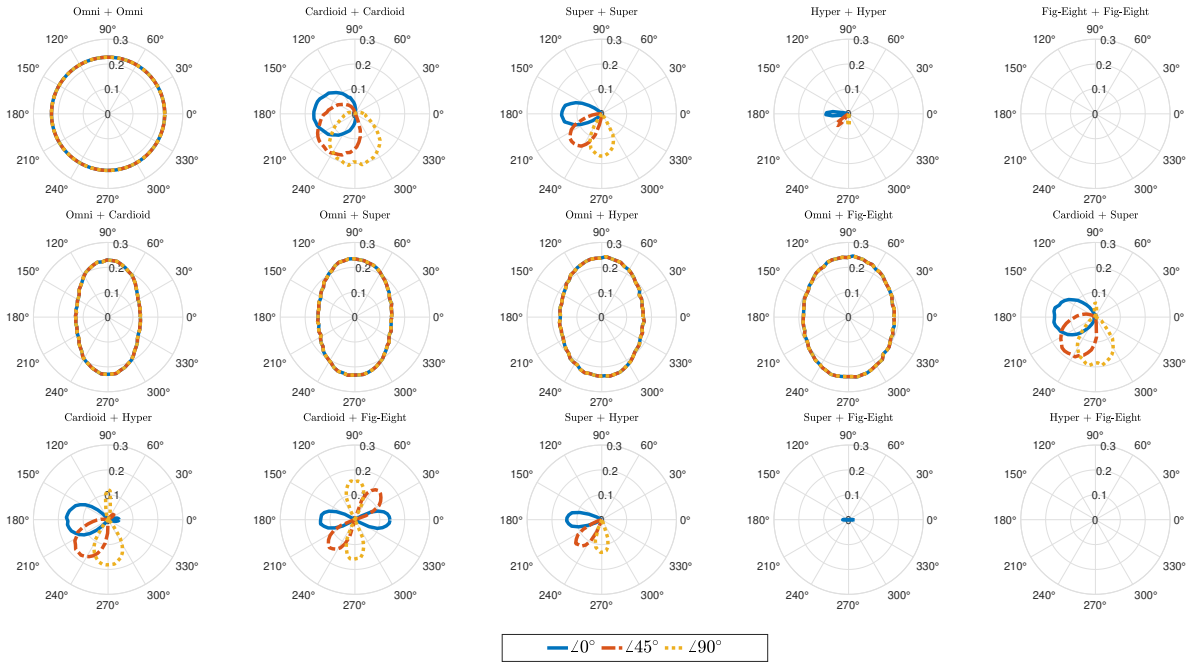

Figure 4: Size of the -10 ***dB estimation zones when the first microphone of each configuration is orientated at*** $0°$***,*** $45°$ ***and*** $90°$ ***and the second is rotated through a full circle.***

optimal observation filter. For a two-microphone system, this is given by

$$\kappa(\boldsymbol{S}_{\text{mm}}) = \frac{\lambda_{\max}}{\lambda_{\min}} = \frac{S_1 + S_2 + \sqrt{(S_1 - S_2)^2 + 4\,|S_{12}|^2}}{S_1 + S_2 - \sqrt{(S_1 - S_2)^2 + 4\,|S_{12}|^2}}, \tag{15}$$

where $\lambda_{\max}$ and $\lambda_{\min}$ are the largest and smallest eigenvalues of $\boldsymbol{S}_{\text{mm}}$. For $\kappa(\boldsymbol{S}_{\text{mm}})$ to attain its minimum value of unity, the two eigenvalues must be equal. Setting their difference to zero and solving we get

$$\lambda_{\max} - \lambda_{\min} = \sqrt{(S_1 - S_2)^2 + 4\,|S_{12}|^2} = 0. \tag{16}$$

At the minimum, both terms under the square root must be zero. From Eq. (13), setting the first term to zero implies that $a_1 = a_2$. This condition follows intuitively since the minimum is achieved for a scaled

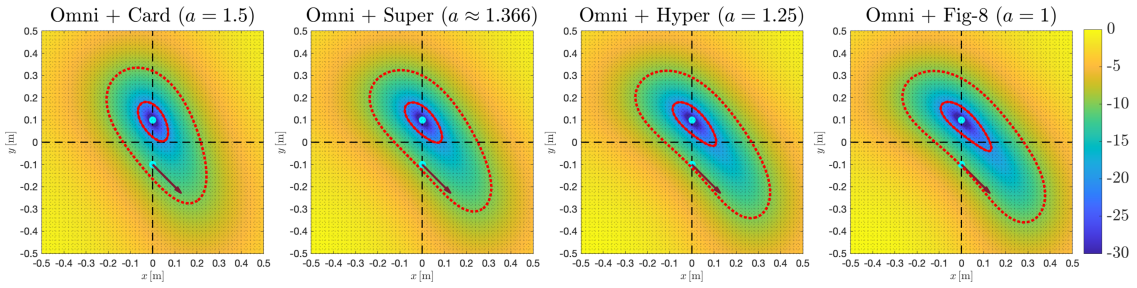

Figure 5: Spatial distribution of the microphone combinations with one directional microphone, rotated to form a $-45°$ ***angle with the*** x***-axis. The sound field frequency is*** $f = 200$ ***Hz. The solid lines (–) denote the area for which*** $L_e \leq -20$ ***dB and the dashed lines (- -) enclose the area where*** $L_e \leq -10$ ***dB.***

identity matrix. However, the value of S_{12} depends on the $b_{\parallel}$ and $b_{\perp}$, which are influenced by the microphone orientations, and on kr through the correlation functions. Therefore, a combination of microphone responses that achieves a unique, frequency-independent global minimum cannot be reached.

To investigate the conditioning of microphone pairs, the condition number, calculated using Eq. (15), is shown in Fig. 6, for all combinations of a_{n} and three microphone orientations: one with the microphones orientated on opposite directions along the array axis, as in Fig. 3, one with the microphones forming a $90°$ angle between themselves and orientated $\pm 45°$ to the x-axis, as in Fig. 5, and one with both microphones orthogonal to the array axis, forming a $0°$ angle with the x-axis. The distance between the microphones for these simulations is reduced to $r = 0.05$ m to exemplify the conditioning.

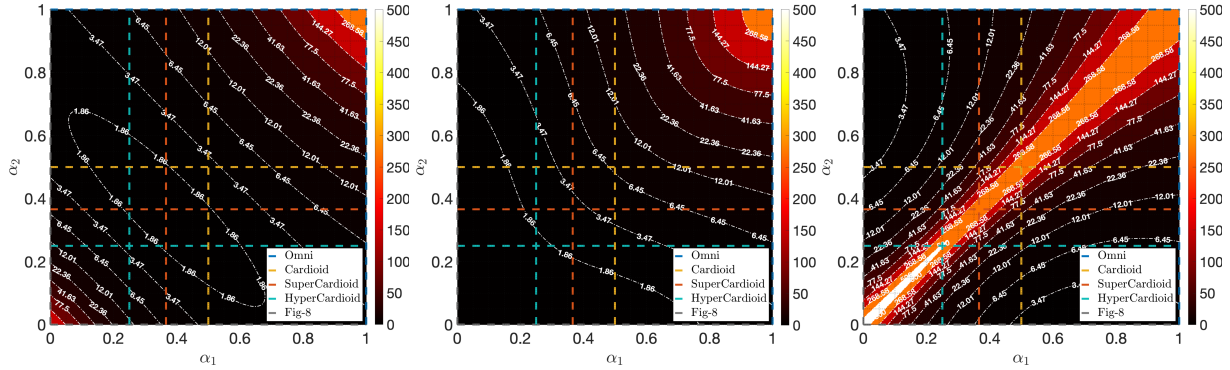

(a) $\theta_1 = 90°$, $\theta_2 = -90°$. *(b)* $\theta_1 = 45°$, $\theta_2 = -45°$. *(c)* $\theta_1 = 0°$, $\theta_2 = 0°$.

Figure 6: Condition number for three different orientations of two microphones $r = 0.05$ ***m apart, estimating a diffuse field of frequency*** $f = 200$ ***Hz. The dash lines denote the*** a ***values associated with the conventional directional microphones.***

Figure 6 shows that the condition number of two omnidirectional microphones is consistently high, as previously reported.[3] When microphones are orientated in opposite directions, a pair of supercardioids achieves the minimum conditioning, as they are designed to maximise the response difference between the front and back sides (*Front-to-Back* ratio), achieving maximum isolation on the direction of the other microphone. For orthogonal orientations, unsurprisingly, the minimum is achieved via the combination of two figure-of-eight microphones, whose responses depend on orthogonal particle velocity components, resulting in zero correlation.[22] These results align with the earlier discussion, where the necessary condition for minimising the condition number was the use of microphones with the same directional response. However, when microphones are orientated in the same direction, arrays with identical microphones exhibit significantly high condition numbers, even surpassing that of the omnidirectional pair. In this case, the particle velocity correlations sum constructively, increasing the total correlation between the microphones. Specifically, for arrays with identical microphones, the system becomes singular as $kr \to 0$. It is important to note that this is not the case if the microphones are not identical, as illustrated in Fig. 6c.

Figure 7 shows the condition number associated with arrays comprising microphones with the same directional responses, for kr values ranging from 0 to 10. The vertical dashed line denotes $kr \approx 0.18$, corresponding to the value resulting from the frequency and microphone distance used in Fig. 6.

It is notable that there are specific kr values at which the condition number for all configurations shown in the figure is the same. As the angle between the microphone particle velocity vectors moves from $180°$ to $0°$, the first kr value at which the condition numbers become identical shifts towards 0. When the microphones are not parallel to the x-axis, directional microphone pairs exhibit a lower condition number compared to the conventional omnidirectional pair for low kr values. However, for kr values higher than the first value at which the condition of the pairs becomes equal, the omnidirectional pair's conditioning

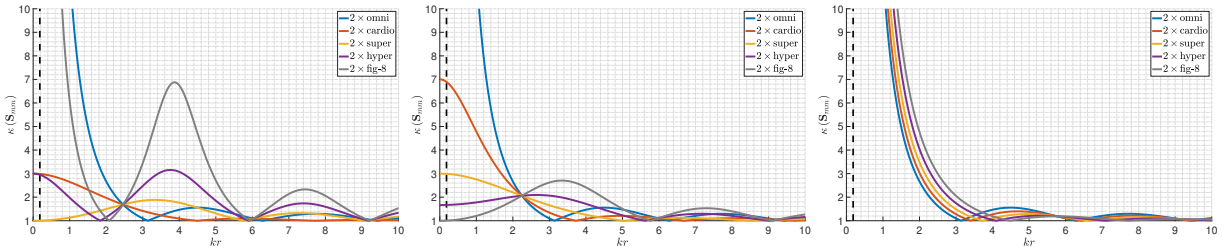

(a) $\theta_1 = 90°$, $\theta_2 = -90°$. *(b)* $\theta_1 = 45°$, $\theta_2 = -45°$. *(c)* $\theta_1 = 0°$, $\theta_2 = 0°$.

Figure 7: Power spectral density matrix condition number for three different orientations of two microphones for various values of kr.

becomes comparable to that of the directional microphone setups. Moreover, higher particle velocity contributions result in more pronounced ripples in the condition number, particularly after the first kr value at which the condition number of the pairs becomes equal.

B. PERFORMANCE AGAINST NOISE

From Eq. (13), it is evident that any pressure weight less than unity reduces the power spectral density of the microphone. For perturbations that diagonally load the power spectral density matrix, $\boldsymbol{S}_{\mathrm{mm}}$, the deviation from the optimal filter will be larger for arrays with smaller values along the main diagonal, such as directional microphones, when compared to conventional omnidirectional pairs. While this does not precisely describe the sensitivity of directional microphones to spatially uncorrelated noise,[17,23] it is explored in this section and serves as an indication of the expected performance reduction exhibited by directional microphones in unfavourable noise conditions.

To evaluate the estimation performance of directional microphones in noisy conditions, the PSD matrices are diagonally loaded with noise of magnitude expressed relative to the output of an ideal pressure sensor, which is normalised to unity in this work. The loading matrix is calculated as

$$\boldsymbol{S}_{\mathrm{n}} = \mu \boldsymbol{I}, \tag{17}$$

where μ represents the signal-to-noise ratio (SNR) relative to the PSD of the omnidirectional microphone. It must be noted that the total noise added to the system is 2μ, meaning that the SNR denotes the noise added to each microphone, not the total system noise. The value of μ for a specified SNR expressed in dB is calculated as

$$\mu = 10^{-\mathrm{SNR}/10}. \tag{18}$$

Figure 8 presents the size of the -10 dB estimation zones for all microphone combinations when the microphones are contaminated with noise, for microphones orientated in opposite directions along the array axis. All other parameters are kept as in Sec. 3. The x symbol in the legend indicates configurations that do not generate an estimation under any SNR condition.

For arrays with identical microphones, reducing the pressure contribution increases the sensitivity to noise and reduces the estimation zone size overall. Arrays comprising a single omnidirectional microphone produce larger estimation zones than most of the other arrays at high SNRs but are more susceptible to noise compared to the conventional omnidirectional pair, failing to generate a zone at SNR levels about 3 dB lower. For these configurations, increasing the particle velocity contribution increases the size of the estimation zone without significantly sacrificing robustness to noise. Arrays with combinations of different directional microphones show significant variability in their performance. As described in Sec. 3, including

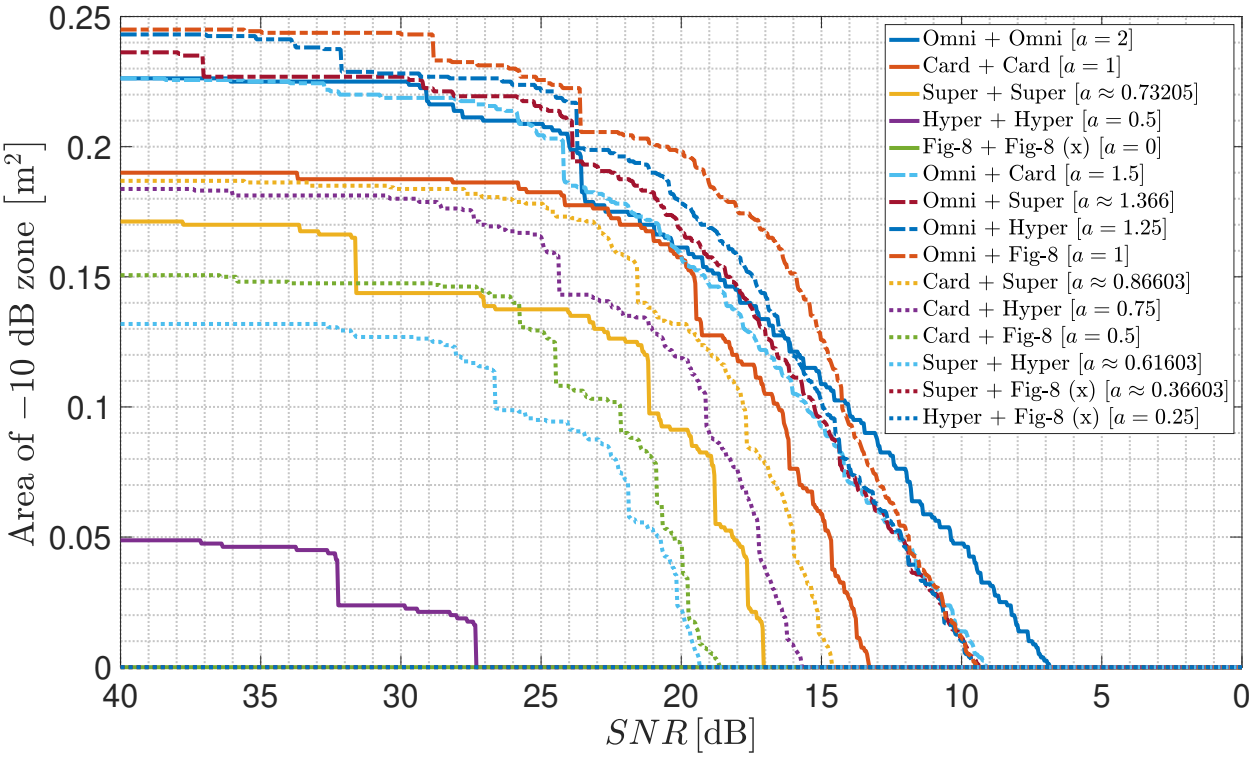

Figure 8: Size of the -10 dB estimation zones when the microphones' responses are contaminated with uncorrelated white noise for microphones orientated in opposite directions along the array axis. The x symbols in the legend indicate pairs that fail to produce an estimation zone under any SNR condition.

a microphone with considerable pressure contribution increases the estimation zone size. This is evident in the figure, where arrays with a cardioid microphone consistently generate larger estimation zones than arrays with mixed directional microphones that do not include a cardioid.

5. SUMMARY

This study presented a preliminary simulation investigation into the estimation performance of two-microphone arrays comprising first-order directional microphones in an ideal diffuse sound field using the Remote Microphone Technique and the analytical formulation of the statistical characteristics of the microphone responses.

The estimation performance of all microphone pair combinations was assessed over a square virtual microphone grid in a tonal diffuse disturbance field. The findings highlight the critical role of localised pressure information in achieving good overall estimation performance. Moreover, it was demonstrated that microphone orientation has a significant impact on the performance of the arrays. Arrays consisting solely of directional microphones achieved good performance only when orientated in opposite directions. Combinations of one omnidirectional and one directional microphone demonstrated good performance at larger distances from the array compared to the conventional omnidirectional array. Furthermore, estimation performance increased near the omnidirectional microphone and extended along the direction of the particle velocity component provided by the directional microphone.

The robustness of the arrays to perturbations was evaluated using the condition number of their power spectral density matrix. At low frequencies, the arrays with combinations of first-order microphones exhib-

ited significantly reduced conditioning compared to the conventional omnidirectional configuration. Arrays comprising two microphones with the same directional response suffered from significant sensitivity when orientated in the same direction. However, when orientated in different directions, their condition number was smaller than the omnidirectional pair at low frequencies. At higher frequencies, these arrays could exhibit higher variability than the conventional array, but the overall conditioning remained consistently low.

The estimation performance was assessed when the microphone responses were contaminated by spatially uncorrelated noise. Combinations of an omnidirectional and a directional microphone achieved good estimation over a larger area than the other configurations. While these combinations exhibited higher sensitivity than the conventional array, the difference was small and became significant only at high noise levels.

These results underscore the importance of microphone orientation and the inclusion of pressure information in achieving robust and accurate estimation performance in virtual sound systems. Future work should explore these findings in more complex acoustic environments, with different and larger microphone arrays and investigate the performance of practical directional microphones.

ACKNOWLEDGMENTS

This work was supported by the project "IN-NOVA: Active reduction of noise transmitted into and from enclosures through encapsulated structures", which has received funding from the European Union's Horizon Europe programme under the Marie Skłodowska-Curie grant agreement no. 101073037 and by UK Research and Innovation under the UK government's Horizon Europe funding agreement with grant number EP/X027767/1. Jordan Cheer was supported by the Department of Science, Innovation and Technology (DSIT) Royal Academy of Engineering under the Research Chairs and Senior Research Fellowships programme.

REFERENCES

[1] D. Prokhorov, "Virtual Sensors and Their Automotive Applications," in *2005 International Conference on Intelligent Sensors, Sensor Networks and Information Processing*, IEEE, Melbourne, Australia (2005), pp. 411–416.

[2] D. Moreau, B. Cazzolato, A. Zander, and C. Petersen, "A Review of Virtual Sensing Algorithms for Active Noise Control," Algorithms **1**(2), 69–99 (2008).

[3] W. Jung, S. J. Elliott, and J. Cheer, "Estimation of the pressure at a listener's ears in an active headrest system using the remote microphone technique," The Journal of the Acoustical Society of America **143**(5), 2858–2869 (2018).

[4] W. Jung, S. J. Elliott, and J. Cheer, "Local active control of road noise inside a vehicle," Mechanical Systems and Signal Processing **121**, 144–157 (2019).

[5] J. Zhang, S. J. Elliott, and J. Cheer, "Robust performance of virtual sensing methods for active noise control," Mechanical Systems and Signal Processing **152**, 107453 (2021).

[6] D. J. Moreau, J. Ghan, B. S. Cazzolato, and A. C. Zander, "Active noise control in a pure tone diffuse sound field using virtual sensing," The Journal of the Acoustical Society of America **125**(6), 3742–3755 (2009).

[7] B. Xu and S. D. Sommerfeldt, "Generalized acoustic energy density based active noise control in single frequency diffuse sound fields," The Journal of the Acoustical Society of America **136**(3), 1112–1119 (2014).

[8] S. Elliott and J. Garcia-Bonito, "Active cancellation of pressure and pressure gradient in a diffuse sound field," Journal of Sound and Vibration **186**(4), 696–704 (1995).

[9] S. D. Sommerfeldt and P. J. Nashif, "An adaptive filtered- x algorithm for energy-based active control," The Journal of the Acoustical Society of America **96**(1), 300–306 (1994).

[10] J. W. Parkins, S. D. Sommerfeldt, and J. Tichy, "Narrowband and broadband active control in an enclosure using the acoustic energy density," The Journal of the Acoustical Society of America **108**(1), 192–203 (2000).

[11] Y. C. Park and S. D. Sommerfeldt, "Global attenuation of broadband noise fields using energy density control," The Journal of the Acoustical Society of America **101**(1), 350–359 (1997).

[12] A. Kappis, J. Cheer, and J. A. Zhang, "Remote Sensing Using Multi-Microphone Configurations for Local Active Noise Control Applications," in *30th International Congress on Sound and Vibration*, Amsterdam, The Netherlands (2024).

[13] H. Li, S. Wang, J. Tao, and X. Qiu, "Enhancing the coherence between virtual and physical signals in virtual sensing with a double-layer microphone arrangement," The Journal of the Acoustical Society of America **157**(4), 2392–2403 (2025).

[14] B. S. Cazzolato and J. Ghan, "Frequency domain expressions for the estimation of time-averaged acoustic energy density," The Journal of the Acoustical Society of America **117**(6), 3750–3756 (2005).

[15] J. W. Parkins, S. D. Sommerfeldt, and J. Tichy, "Error analysis of a practical energy density sensor," The Journal of the Acoustical Society of America **108**(1), 211–222 (2000).

[16] B. Cazzolato and C. Hansen, "Errors Arising from Three-Dimensional Energy Density Sensing in One-Dimensional Sound Fields," Journal of Sound and Vibration **236**(3), 375–400 (2000).

[17] M. Brandstein, D. Ward, A. Lacroix, and A. Venetsanopoulos, eds., *Microphone Arrays: Signal Processing Techniques and Applications*, Digital Signal Processing (Springer Berlin Heidelberg, Berlin, Heidelberg, 2001).

[18] M. Kuster, "Spatial correlation and coherence in reverberant acoustic fields: Extension to microphones with arbitrary first-order directivity," The Journal of the Acoustical Society of America **123**(1), 154–162 (2008).

[19] S. J. Elliott and J. Cheer, "Modeling local active sound control with remote sensors in spatially random pressure fields," The Journal of the Acoustical Society of America **137**(4), 1936–1946 (2015).

[20] S. J. Elliott, J. Cheer, J.-W. Choi, and Y. Kim, "Robustness and Regularization of Personal Audio Systems," IEEE Transactions on Audio, Speech, and Language Processing **20**(7), 2123–2133 (2012).

[21] P. Zhang, S. Wang, H. Duan, J. Tao, H. Zou, and X. Qiu, "A study on coherence between virtual signal and physical signals in remote acoustic sensing," The Journal of the Acoustical Society of America **152**(5), 2840–2848 (2022).

[22] F. Jacobsen, "The diffuse Sound Field - Statistical Considerations Concerning the Reverberant Field in the Steady State," 27, Technical University of Denmark, Denmark (1979).

[23] J. Chen, J. Benesty, and C. Pan, "On the design and implementation of linear differential microphone arrays," The Journal of the Acoustical Society of America **136**(6), 3097–3113 (2014).